

FitController: Toward Fit-Aware Virtual Try-On

Lu Yang¹ Yicheng Liu¹ Yanan Li² Xiang Bai¹ Hao Lu^{1,✉}

¹Huazhong University of Science and Technology ²Wuhan Institute of Technology

{lu-yang1, light76, xbai, hlu✉}@hust.edu.cn yananli@wit.edu.cn



Figure 1. **Illustrations of FitController generations.** We present FitController, a plug-in module for diffusion-based virtual try-on models that enable customized control of the garment fit. Zoom in and compare contour differences.

Abstract

Realistic virtual try-on (VTON) concerns not only faithful rendering of garment details but also coordination of the style. Prior art typically pursues the former, but neglects a key factor that shapes the holistic style—garment fit. Garment fit delineates how a garment aligns with the body of a wearer and is a fundamental element in fashion design. In this work, we introduce fit-aware VTON and present FitController, a learnable plug-in that can seamlessly integrate into modern VTON models to enable customized fit control. To achieve this, we highlight two challenges: i) how to delineate layouts of different fits and ii) how to render the garment that matches the layout. FitController first features a fit-aware layout generator to redraw the body-garment layout conditioned on a set of delicately processed garment-agnostic representations, and a multi-scale fit injector is then used to deliver layout cues to enable layout-driven VTON. In particular, we build a fit-aware VTON dataset termed Fit4Men, including 13,000 body-garment pairs of different fits, covering both tops and bottoms, and featuring varying camera distances and body poses. Two fit consistency metrics are also introduced to assess the fitness of generations. Extensive experiments show that FitController can work with various VTON models and achieve accurate fit control. Code and data will be released.

1. Introduction

“*Does this outfit suit me?*”—this is a common question for online shoppers, yet difficult to answer through imagination alone. VTON seeks to bridge this gap by generating realistic try-on images of a wearer with desired garments. Realistic VTON generation, however, is difficult. It hinges on not only faithful preservation of garment appearance and body pose but also coordination of the holistic style. Existing work [4–6, 17, 37, 51] mainly focuses on recovering garment details while overlooking the style consistency. Per Fig. 2(a), this negligence can result in disharmony of the feeling and may mismatch user preferences.

In the fashion domain, style is primarily influenced by three factors: color coordination, ways of wearing, and fit [20, 46]. Since the garment is preset, the latter two matter in VTON. Ways of wearing—such as tucking in the hem or rolling up sleeves—affect local styles, while *fit shapes the holistic style*, delineates how a garment aligns with the body, and is governed by physical factors such as garment proportions, measurements, and ease allowance. These physical properties manifest visually via variations in tightness (e.g., slim vs. loose T-shirts) and shape (e.g., tapered vs. straight trousers) [46], making it possible to reproduce target fits visually without the need for precise physical modeling.

In this work, we introduce fit-aware VTON and present FitController, a novel plug-in engineered for seamless integration with modern diffusion-based VTON models, empowering users with customized fit control (Fig. 2(b)). We remark that a key challenge for fit-aware VTON lies in *how to ground the abstract notion of fit into tangible visual representations*. To this end, FitController follows a two-stage design: i) delineating the spatial layout between the garment and body given a certain fit, and ii) rendering the garment onto the body conditioned on the layout.

The first stage deals with spatial modeling between the body and garment. Following [4, 45], we use the segmentation map to represent the body-garment layout and introduce a fit-aware layout generator to redraw the target segmentation map conditioned on the fit label. During layout generation, a phenomenon called *garment shape leakage* arises. This leads to a problem where the generator is biased toward replicating the original garment shape, instead of generating a new one. To address this, we redesign the garment-agnostic representation preprocessor to produce a rectangular mask and a dense pose conditioned on body proportions. The second stage follows a conditional image generation pipeline. Unlike previous approaches [28, 47] that often rely on an extra encoder to extract conditional image features, we repurpose the features from the layout generator, and a lightweight multi-scale fit injector is used to deliver the layout features to off-the-shelf VTON models via the ControlNet [47] interface. We find that such a simplification not only reduces the computational overhead but also accelerates training convergence.

In particular, we harvest a fit-orientated VTON dataset, termed Fit4Men. We focus on men garments because they feature limited but well-defined garment styles compared with more varied women garments, making them suitable for an initial exploration on this topic. Fit4Men features 5,000 pairs of men T-shirts with *slim*, *regular*, and *loose* fits and 8,000 pairs of men trousers with *tapered* and *straight* fits. The dataset covers diverse body poses and varying camera distances. To objectively assess the fitness of try-on generations, two fit consistency metrics measuring contour differences are also introduced.

Experiments demonstrate that FitController can be incorporated into various VTON architectures, providing precise control over garment fit while enhancing the perceptual quality of try-on generations. Ablation studies further show that effective fit control can be achieved with as few as 1,000 training steps or with only 1,000 training samples, highlighting good training and sample efficiency.

To our knowledge, our work is the first attempt that systematically investigates fit-aware VTON, from data and methods to metrics and design considerations, which charts a path toward accurate fit control over diverse garments with VTON models.

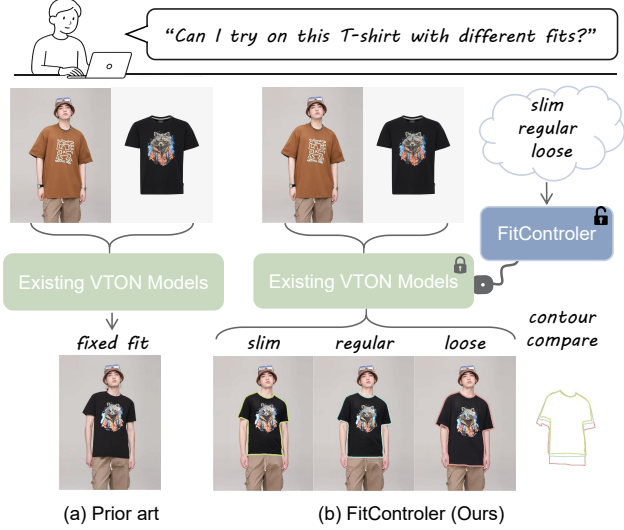


Figure 2. **Comparison between existing VTON models and our proposed FitController.** (a) Existing models produce only a fixed fit, often leading to unnatural results due to mismatched fit. (b) With FitController, the same inputs can produce try-on results with customized fits such as *slim*, *regular*, and *loose* T-shirts, which better matches the overall style and user preference.

2. Related Work

Our work is related to image-based VTON, customized VTON, and controllable image generation.

Image-based Virtual Try-On. Image-based VTON aims to transfer a target garment onto a person and synthesize photorealistic try-on images. Conventional methods [4, 11, 22, 38, 45] typically follow a two-stage pipeline by i) warping the garment to align with the target human pose and ii) compositing try-on images using a generative model [8]. These approaches, however, can suffer from poor geometric warping under large deformations and unrealistic garment rendering due to the limited generation quality.

Recent diffusion-based methods leverage attention operations to model garment-person interactions, reducing reliance on explicit warping. They differ mainly in how garment details are captured. For instance, LaDI-VTON [27] and DCI-VTON [9] encode garments using CLIP [35], but CLIP embeddings fail to preserve fine-grained textures due to their focus on high-level semantics. To address this, StableVITON [17] employs a ControlNet-like [47] architecture to capture garment features, enhancing detail preservation. Following TryOnDiffusion [52], mainstream approaches [5, 15, 37, 40, 51] repurpose the denoising backbone to extract garment features, further improving texture fidelity. Although effective, this dual-branch design significantly increases training and inference costs. TPD [43] and CatVTON [6] streamline the pipeline by jointly encoding garment and person features within a single U-Net, boosting

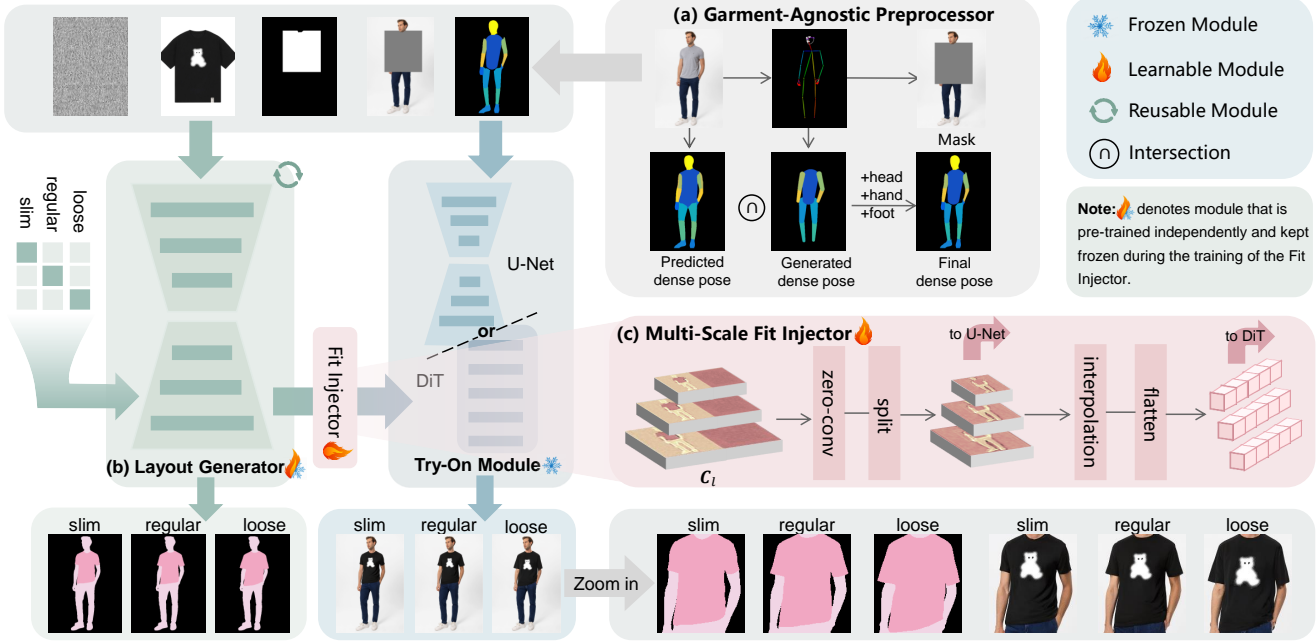


Figure 3. **Overview of FitController.** The person image is first processed by (a) the *garment-agnostic preprocessor* to extract the mask and dense pose. These are concatenated with the noise map and garment image—along both channel and spatial dimensions as in CatVTION [6]—before being fed into (b) the *fit-aware layout generator* to produce a fit-sensitive segmentation map. The layout features are then delivered by (c) the *multi-scale fit injector* to VTON models via the ControlNet [47] interface. The layout generator is pre-trained and remains frozen when integrating FitController into different VTON models, where only the fit injector requires model-specific training.

both efficiency and fidelity. Despite these advances, they overlook the wearing style, often leading to unnatural results. In particular, the inconsistency of garment fit—such as mismatched tightness between tops and bottoms—can significantly degrade realism. To address this, we explicitly model the garment fit to enable fit-aware VTON.

Customized Virtual Try-On. Due to personalized demands, some work has also explored customized VTON. For instance, landmark-based methods [2, 3, 23, 42] enable the control over local wearing styles such as rolling up sleeves or tucking in hems. Text-based methods [18, 24, 53] generate try-on images from textual descriptions, offering potential attribute control. However, the controllability of these approaches is mainly applicable to specific model architectures—even text-based control cannot be applied to all diffusion-based models (*e.g.*, CatVTION [6] drops text input). In this work, we consider garment fit as a holistic attribute and design a plug-in for modern diffusion-based VTON models.

Controllable Image Generation. Recently, notable progress in controllable image generation [34, 41, 50] has enabled conditional guidance such as segmentation maps, canny edges, or depth maps, without retraining text-to-image diffusion models [29, 30, 36]. For example, ControlNet [47] only trains an auxiliary encoder mirroring

the structure of the denoising model, and T2I-Adapter [28] introduces a lightweight network for the same purpose. These methods, however, focus solely on guiding generation from a conditional image, without considering how the condition is acquired. As a result, they typically feature an additional encoder to process the conditional input. In contrast, our approach generates the conditional image itself, allowing us to repurpose features from the generator, which simplifies model design and improves efficiency.

3. FitController

We begin with the problem setup and then present technical details of FitController.

3.1. Problem Setup

Given a person image \mathbf{x}_p and a garment image \mathbf{x}_g , fit-aware VTON aims to synthesize a try-on image \mathbf{x}_{tr} according to a target fit prompt \mathbf{l} , where $\mathbf{x}_p, \mathbf{x}_g, \mathbf{x}_{tr} \in \mathbb{R}^{H \times W \times 3}$, with H being the image height and W the image width, and \mathbf{l} can be of various forms, such as text or categorical labels.

A common paradigm [3, 18] is to design a dedicated try-on model \mathcal{T} that accepts \mathbf{l} as an additional input such that

$$\mathbf{x}_{tr} = \mathcal{T}(\mathcal{P}(\mathbf{x}_p), \mathbf{x}_g, \mathbf{l}), \quad (1)$$

where $\mathcal{P}(\mathbf{x}_p)$ is a preprocessor that generates garment

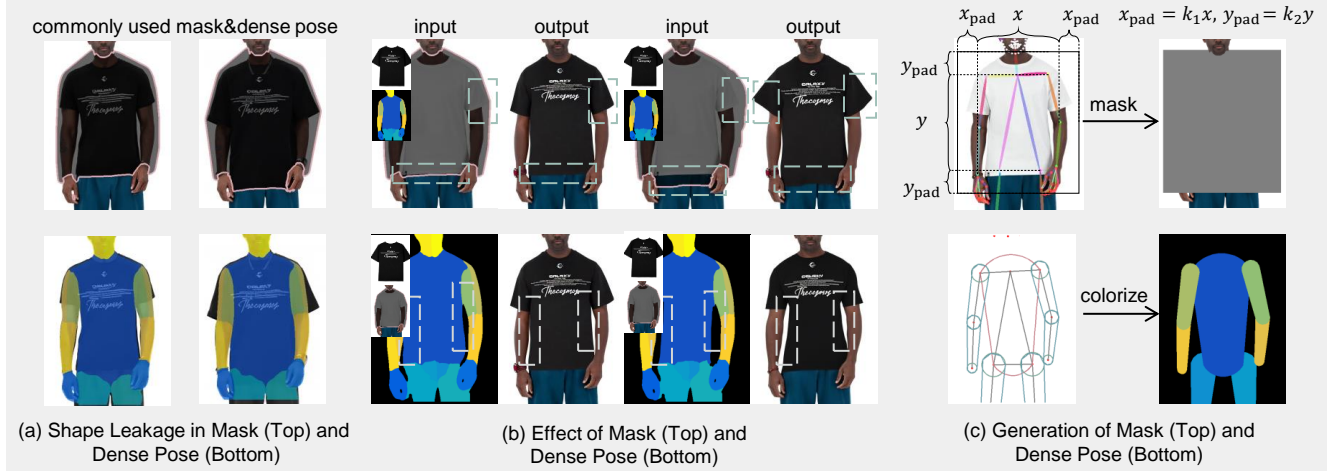


Figure 4. **Impact of shape leakage in mask and dense pose.** (a) Commonly used masks and dense poses implicitly encode the original garment boundaries, which (b) biases the model to follow these cues when rendering garment. To address this, (c) our preprocessor reconstructs them from human keypoints to form standardized representations. See supplementary material for the ablation on this preprocessor.

agnostic representations (e.g., masked images) [4] from x_p . This paradigm, however, tightly couples the fit control mechanism with a certain model and cannot easily integrate into other VTON models.

Unlike the common paradigm, our idea is to design a plug-in \mathcal{F} that is compatible with existing VTON models. This requires addressing two key problems: i) how to encode the fit prompt l into the fit feature C_l with clear fit awareness and ii) how to enable try-on models to effectively decode C_l . We formulate the two problems as

$$C_l = \mathcal{F}(\mathcal{P}(x_p), x_g, l), \quad (2)$$

$$x_{tr} = \mathcal{T}(\mathcal{P}(x_p), x_g, C_l). \quad (3)$$

3.2. FitController Overview

Fig. 3 shows the technical pipeline of FitController. FitController instructs the fit with categorical labels and features i) a *garment-agnostic preprocessor* utilizing human keypoints and body proportions to generate a square-shaped mask and a simulated dense pose; ii) a *fit-aware layout generator* producing the fit feature that encodes the body-garment spatial relation, conditioned on the fit label; and iii) a *multi-scale fit injector* mapping the fit feature compatible with try-on models and injects it via the ControlNet [47] interface.

3.3. Garment-Agnostic Preprocessor

Garment-agnostic representations are standard inputs to VTON models that aim to reduce the cost of data collection. They enable training with (garment, try-on image) pairs under reconstruction-based supervision. However, commonly used representations such as the mask and the dense pose (Fig. 4(a)) often preserve the original garment contour, because the mask is typically generated along the garment

boundary, and DensePose [10] tends to misinterpret garment edges as body boundaries. Consequently, the model is biased to render garments following these leaked cues (Fig. 4(b)), indicating that the standard representations do not meet the need of fit-aware synthesis. To address this, we redesign the garment-agnostic preprocessor $\mathcal{P}(x_p)$ to eliminate garment shape leakage.

Mask. Unlike prior work [4] that estimates masks from detected garment regions, we derive masks from human keypoints to avoid garment contour leakage. Specifically, for the upper body, we define x as the horizontal span between the minimum and maximum coordinates of the shoulder, elbow, and wrist joints, and y as the vertical span between the shoulder and hip keypoints. The mask is generated as in Fig. 4(c), where two empirical padding ratios $k_1 = 0.6$ and $k_2 = 0.25$ to fully cover the clothing region while minimizing unnecessary background. For the lower body, we construct the mask based on the hip, knee, and ankle keypoints, with $k_1 = 0.5$ and $k_2 = 0.2$.

DensePose. To mitigate inaccuracies in the predicted dense pose, we synthesize a standard-stature dense pose based on human keypoints and canonical body proportions. According to Fig. 4(c), the torso is approximated by a quadrilateral defined by shoulder and hip joints, with convex arcs at the top and bottom to yield natural contours. Limbs are constructed by connecting circles placed at major joints (shoulder–elbow–wrist and hip–knee–ankle), whose diameters are proportional to body height (e.g., 0.06, 0.048, 0.033 for the arm; 0.09, 0.055, 0.03 for the leg). Body height is estimated to be of $3.2 \times$ torso height or $2.3 \times$ leg length. Finally, the synthesized map is intersected with the predicted dense pose to constrain the spatial layout.

3.4. Fit-Aware Layout Generator

The fit-aware layout generator produces a body-garment layout conditioned on the fit label \mathbf{l} . We represent the layout as a segmentation map and repurpose the U-Net from Stable Diffusion [36] to achieve this task. The rich semantic priors from the pretrained U-Net can benefit layout prediction.

Formally, given a person image \mathbf{x}_p and a garment image \mathbf{x}_g , we first derive the mask \mathbf{m} , the masked person image \mathbf{x}_m , and the dense pose \mathbf{x}_d via $\mathcal{P}(\mathbf{x}_p)$. Since the U-Net operates in the latent space of a VAE [19], these inputs are first encoded by the VAE encoder $\mathcal{E}(\cdot)$, with the mask \mathbf{m} downsampled to the corresponding resolution. A Gaussian noise map \mathbf{z}_T is further sampled as the stochastic input. The input to the generator is a 13-channel tensor

$$\mathcal{X} = \mathbf{z}_T \parallel [\mathbf{m} \oplus \mathbf{0}] \parallel [\mathcal{E}(\mathbf{x}_m) \oplus \mathcal{E}(\mathbf{x}_g)] \parallel [\mathcal{E}(\mathbf{x}_d) \oplus \mathbf{0}], \quad (4)$$

along with the one-hot encoded fit label \mathbf{l} , where $\mathbf{0}$ is a zero tensor used for spatial alignment, \oplus denotes spatial concatenation, and \parallel channel-wise concatenation, following CatVT-
TON [6]. Then the layout generator \mathcal{G}_S produces

$$\mathcal{S}_l, \mathbf{C}_l = \mathcal{G}_S(\mathcal{X}, \mathbf{l}), \quad (5)$$

where \mathcal{S}_l is a three-class segmentation map (background, body, and garment), and \mathbf{C}_l is the fit-aware features aggregated from multi-scale intermediate decoder features before ResNet blocks. To condition \mathbf{l} , we follow the prior controlled image generation pipeline [30, 33] and inject it through feature-level modulation using FiLM [31] in each ResNet block of the decoder, which amounts to

$$\mathbf{h}_s \leftarrow \gamma(\mathbf{l}) \cdot \frac{\mathbf{h}_s - \mu}{\sigma} + \beta(\mathbf{l}), \quad (6)$$

where \mathbf{h}_s denotes intermediate features, μ and σ are feature-wise statistics, and $\gamma(\cdot)$ and $\beta(\cdot)$ are learnable projections. Notably, we freeze the U-Net encoder to preserve its pretrained semantic knowledge. Additional implementation details are provided in the supplementary material.

3.5. Multi-Scale Fit Injector

The fit injector transforms the multi-scale layout features \mathbf{C}_l into a compatible representation that is acceptable by VTON models.

At each scale, a zero-initialized convolution layer is first applied to align the layout features with try-on features. To ensure spatial consistency, we apply operations such as splitting and interpolation to match the resolution of the try-on model. For U-Net based models (e.g., Leffa [51]), resolution alignment can be achieved by simple splitting operations. In contrast, DiT-based models (e.g., FitDiT [15]) require interpolated feature maps of a uniform resolution, followed by flattening.

During the training of the injector, both the layout generation module and the try-on module remain frozen, and only the injector parameters are optimized using the loss

$$\mathcal{L} = \mathbb{E}_{\zeta, t, \epsilon, \mathbf{C}_l} \left[\|\epsilon - \epsilon_\theta(\zeta, t, \tau_\phi(\mathbf{C}_l))\|_2^2 \right], \quad (7)$$

where τ_ϕ is the injector, t is the diffusion timestep, ϵ is the noise, and ζ denotes the try-on input. For example, in Leffa, $\zeta = [\mathcal{E}(\mathbf{x}_g), \mathbf{z}_t \parallel \mathcal{E}(\mathbf{x}_m) \parallel \mathcal{E}(\mathbf{x}_d) \parallel \mathbf{m}]$.

4. Fit Consistency Metric

Evaluating how well a try-on image adheres to a specific fit is non-trivial, because fit differences manifest in not only realism but also subtle garment contours. This requires explicit contour-aware metrics to compare fit consistency. Concretely, for each source image, we generate a try-on image conditioned on the same fit label, extract the garment contours from both, and measure their similarity. We adopt two complementary shape metrics: Hu moments (Hu) [13] and Hausdorff distance (Hd) [14].

Hu Moments. Hu delineates the shape globally. Given a binary contour mask $I(x, y)$, the central moment of order (p, q) is first computed by

$$\mu_{pq} = \sum_x \sum_y (x - \bar{x})^p (y - \bar{y})^q I(x, y), \quad (8)$$

where (\bar{x}, \bar{y}) is the centroid. It is then normalized to

$$\eta_{pq} = \frac{\mu_{pq}}{\mu_{00}^r}, \quad r = \frac{p+q}{2} + 1. \quad (9)$$

Hu takes the form $\Phi(I) = [\phi_1, \dots, \phi_7]$, where each ϕ_i is a specific combination of η_{pq} 's, e.g., $\phi_1 = \eta_{20} + \eta_{02}$. Hu captures the spatial distribution of contour pixels via moment statistics, providing a compact yet informative representation of global shape. In practice, we compute the Hu distance between two images as a single scalar. The closer the distance between $\Phi(I_{\text{gen}})$ and $\Phi(I_{\text{src}})$ is, the better the garment contour matches, where I_{gen} and I_{src} refer to the generated and source contours, respectively.

Hausdorff Distance. Hd captures local geometric deviations. Given two contour point sets A and B , the Hausdorff distance $d_H(A, B)$ between A and B takes the form

$$d_H(A, B) = \max \left\{ \sup_{a \in A} \inf_{b \in B} d(a, b), \sup_{b \in B} \inf_{a \in A} d(b, a) \right\}, \quad (10)$$

where $d(a, b)$ is the Euclidean distance between points a and b in our case. Hd measures the maximum nearest-neighbor distance between contour points, highlighting mismatches such as the misalignment of sleeve or hem.

With Hu and Hd, our fit consistency metrics take both global shape coherence and local fidelity into account. Lower values of both metrics indicate better performances.

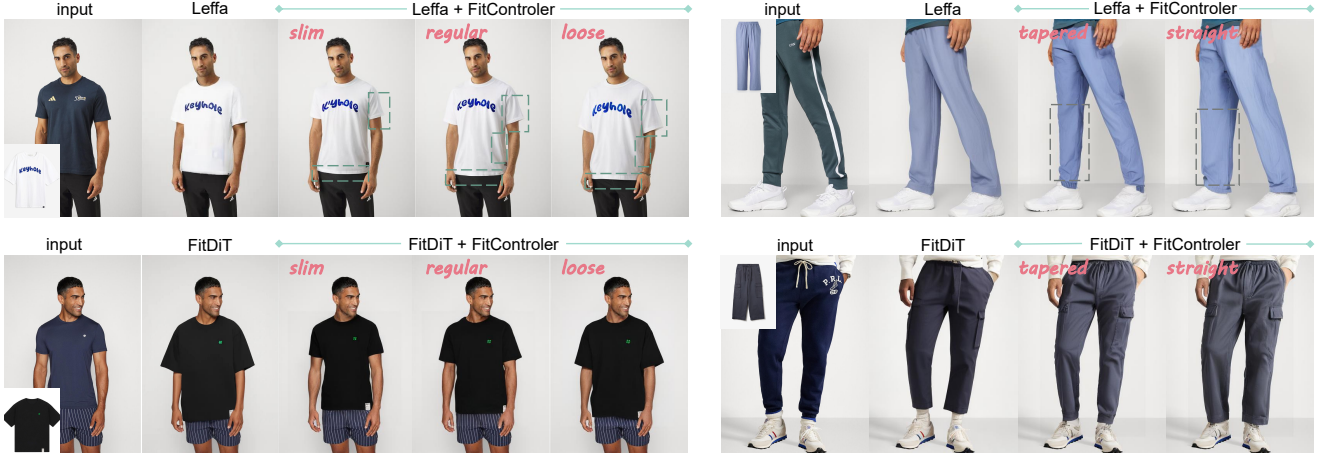


Figure 5. **Qualitative results of VTON models with FitController.** Regions showing the most prominent fit variations are highlighted with dashed boxes. Additional examples on other VTON models are provided in the supplementary material.

Table 1. Analysis of fit consistency metrics. **pd** is the generated image, and **gt** the source image. Best performance is in **boldface**.

| pd | gt | slim | | regular | | loose | |
|---------|----|-------------|-------------|-------------|-------------|-------------|-------------|
| | | Hu | Hd | Hu | Hd | Hu | Hd |
| slim | | 0.32 | 6.46 | 0.43 | 7.60 | 0.67 | 14.34 |
| regular | | 0.41 | 7.65 | 0.39 | 6.35 | 0.54 | 11.16 |
| loose | | 0.58 | 11.61 | 0.47 | 9.24 | 0.43 | 7.34 |

5. Results and Discussion

Here we present our dataset, results, and discussion.

5.1. Experimental Setup

Dataset. Due to the absence of fit-aware VTON dataset, we introduce Fit4Men, a medium-resolution (768×1024) dataset featuring 5,000 pairs of men’s short-sleeve T-shirts and 8,000 pairs of men’s trousers collected from e-commerce platforms.¹ T-shirts are labeled with three fit types (slim, regular, and loose), and trousers with two (tapered and straight). The number of sample pairs is balanced across different fits. The dataset encompasses diverse camera distances and model poses. Further details are provided in the supplementary material.

Implementation Details. We first train the layout generator using the cross-entropy loss. Subsequently, for each try-on model, the fit injector is trained for 7,500 steps following the configuration described in Sec. 3.5. All models are optimized using AdamW [25] with a batch size of 64 and a learning rate of 1×10^{-5} . Training and evaluation are performed at 384×512 resolution with FP16 precision on four NVIDIA A6000 GPUs. Additional training details are provided in the supplementary material.

¹Zalando, Taobao, and Musinsa

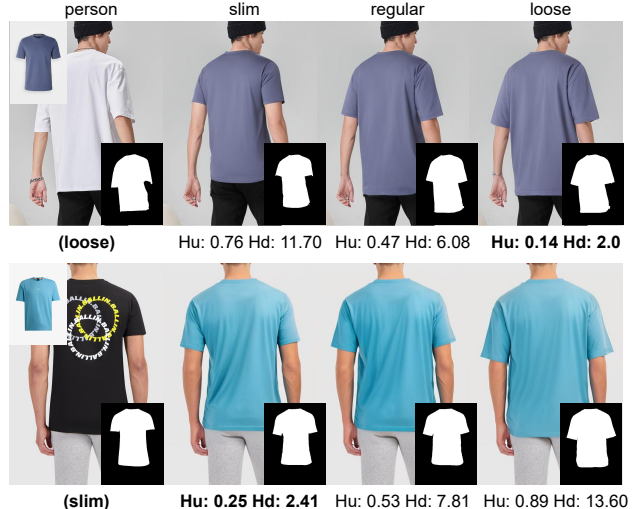


Figure 6. **Correlation analysis of fit consistency metrics.** For each target fit, three types of fits (slim, regular, and loose) are generated and compared.

Experimental Protocol. To demonstrate generality, we integrate FitController into five state-of-the-art VTON models: StableVITON [17], IDM-VTON [5], CatVTON (and its FLUX variant) [6], Leffa [51], and FitDiT [15], covering diffusion backbones from SD1.5 [36] and SDXL [32] to SD3 [7] and FLUX.1 [21]. Each model is evaluated on Fit4Men with and without FitController, under both paired and unpaired settings. The baseline VTON models use their developed preprocessing pipelines for generating garment-agnostic representations. Following prior work [6, 49], we also report FID [12], KID [1], SSIM [39], and LPIPS [48] to assess image quality in the paired setting, and FID/KID in the unpaired setting. Both settings also report Hu and Hd to evaluate fit consistency.

Table 2. Performance of VTON models with/without FitController on Fit4Men. Relative improvements are colored in red \uparrow and green \downarrow .

| Method | Paired | | | | | | Unpaired | | | |
|---------------------|----------------------|---------------------|---------------------|-----------------------|---------------------|---------------------|----------------------|---------------------|---------------------|----------------------|
| | FID \downarrow | KID \downarrow | SSIM \uparrow | LPIPS \downarrow | Hu \downarrow | Hd \downarrow | FID \downarrow | KID \downarrow | Hu \downarrow | Hd \downarrow |
| Short-sleeve | | | | | | | | | | |
| StableVITON [17] | 16.93 | 4.34 | 0.853 | 0.0653 | 0.57 | 9.90 | 21.97 | 5.75 | 0.66 | 10.35 |
| +FitController | 14.39 (15.0%) | 2.53 (41.7%) | 0.874 (2.5%) | 0.0634 (2.9%) | 0.42 (26.3%) | 7.63 (22.9%) | 19.96 (9.1%) | 4.81 (16.3%) | 0.50 (24.2%) | 8.54 (17.5%) |
| IDMVTON [5] | 15.99 | 2.90 | 0.852 | 0.0647 | 0.55 | 9.03 | 20.83 | 3.37 | 0.67 | 10.39 |
| +FitController | 14.69 (8.1%) | 1.92 (33.8%) | 0.866 (1.6%) | 0.0592 (8.5%) | 0.45 (18.2%) | 7.54 (16.5%) | 19.11 (8.3%) | 2.19 (35.0%) | 0.51 (23.9%) | 8.81 (15.2%) |
| CatVTON [6] | 14.28 | 2.02 | 0.864 | 0.0574 | 0.57 | 9.17 | 19.09 | 3.35 | 0.64 | 10.58 |
| +FitController | 13.01 (8.9%) | 1.06 (47.5%) | 0.873 (1.0%) | 0.0552 (3.8%) | 0.44 (22.8%) | 7.13 (22.2%) | 18.29 (4.2%) | 2.07 (38.2%) | 0.49 (23.4%) | 8.64 (18.3%) |
| CatVTON-FLUX [6] | 15.76 | 2.54 | 0.855 | 0.0764 | 0.56 | 9.41 | 20.40 | 3.04 | 0.65 | 10.56 |
| +FitController | 14.44 (8.4%) | 1.39 (45.3%) | 0.860 (0.6%) | 0.0652 (14.7%) | 0.44 (21.4%) | 7.92 (15.8%) | 18.40 (9.8%) | 1.93 (36.5%) | 0.47 (27.7%) | 8.47 (19.8%) |
| FitDiT [15] | 17.40 | 4.17 | 0.864 | 0.0723 | 0.65 | 12.36 | 23.94 | 6.82 | 0.80 | 16.89 |
| +FitController | 12.51 (28.1%) | 0.90 (78.4%) | 0.875 (1.3%) | 0.0510 (29.5%) | 0.38 (41.5%) | 6.77 (45.2%) | 18.48 (22.8%) | 1.86 (72.7%) | 0.46 (42.5%) | 7.94 (53.0%) |
| Leffa [51] | 14.59 | 1.03 | 0.861 | 0.0668 | 0.56 | 9.18 | 18.77 | 2.59 | 0.65 | 10.47 |
| +FitController | 12.45 (14.7%) | 0.62 (39.8%) | 0.869 (0.9%) | 0.0530 (20.7%) | 0.40 (28.6%) | 7.05 (23.2%) | 17.73 (5.5%) | 1.54 (40.5%) | 0.45 (30.8%) | 7.65 (26.9%) |
| Trousers | | | | | | | | | | |
| IDMVTON [5] | 15.11 | 6.67 | 0.854 | 0.0677 | 1.03 | 10.53 | 16.12 | 5.59 | 1.58 | 12.58 |
| +FitController | 12.14 (19.7%) | 3.68 (44.8%) | 0.862 (0.9%) | 0.0592 (12.6%) | 0.81 (21.4%) | 9.32 (11.5%) | 14.43 (10.5%) | 3.95 (29.3%) | 1.13 (28.5%) | 10.29 (18.2%) |
| CatVTON [6] | 11.46 | 3.43 | 0.852 | 0.0637 | 0.92 | 9.50 | 14.19 | 3.94 | 1.48 | 11.92 |
| +FitController | 10.02 (12.6%) | 1.82 (46.9%) | 0.867 (1.8%) | 0.0582 (8.6%) | 0.80 (13.0%) | 8.71 (8.3%) | 12.22 (13.0%) | 1.96 (50.2%) | 1.03 (30.4%) | 9.39 (21.2%) |
| CatVTON-FLUX [6] | 13.81 | 5.61 | 0.844 | 0.0811 | 1.26 | 13.38 | 16.87 | 7.34 | 1.67 | 15.44 |
| +FitController | 12.15 (12.0%) | 4.13 (26.4%) | 0.851 (0.8%) | 0.0796 (1.9%) | 0.91 (27.8%) | 9.49 (29.0%) | 15.42 (8.6%) | 6.42 (12.5%) | 1.19 (28.7%) | 10.78 (30.2%) |
| FitDiT [15] | 14.00 | 4.32 | 0.841 | 0.0832 | 1.26 | 13.36 | 15.74 | 4.30 | 1.86 | 17.49 |
| +FitController | 9.94 (28.9%) | 1.91 (55.7%) | 0.868 (3.1%) | 0.0593 (28.7%) | 0.75 (40.5%) | 7.59 (43.1%) | 12.67 (19.5%) | 2.39 (44.4%) | 1.00 (46.2%) | 8.90 (49.1%) |
| Leffa [51] | 10.56 | 3.27 | 0.850 | 0.0720 | 1.17 | 10.39 | 12.55 | 4.03 | 1.31 | 10.63 |
| +FitController | 9.83 (6.9%) | 1.90 (41.9%) | 0.864 (1.6%) | 0.0610 (15.3%) | 0.74 (36.8%) | 7.87 (24.3%) | 11.98 (4.5%) | 2.12 (47.4%) | 0.98 (25.2%) | 8.80 (17.2%) |

5.2. Sanity Check on Fit Consistency Metrics

Before reporting Hu and Hd, we first perform a sanity check to confirm their soundness in assessing fit consistency. We analyze both qualitative and quantitative results on short-sleeve T-shirts. For the qualitative analysis, we generate three different fits from a person-garment pair and compute the Hu and Hd values relative to the original image (Fig. 6). For the quantitative analysis, we partition the test set into three subsets according to their fit labels and generate VTON results w.r.t. the three different fits for each subset. According to Fig. 6 and Table 1, both metrics achieve the best values when the generated fit matches the original one, and increase progressively with larger fit differences (e.g., loose vs. slim). This confirms Hu and Hd are suitable for evaluating fit consistency.

5.3. Main Results

Here we compare the performance of state-of-the-art VTON models with and without FitController on the Fit4Men dataset. Since StableVITON [17] provides pretrained weights only for upper-body data, it is only evaluated on the short-sleeve subset. Quantitative results are shown in Table 2. One can observe that FitController consistently improves the fit consistency metrics in both Hu and Hd. Interestingly, improved garment fits also lead to consistently im-

proved performance over other image quality metrics (FID, KID, SSIM, and LPIPS), which suggests that fit is an essential factor in achieving realism, but has been underexplored in previous works. Notably, as discussed in Section 3.3, models such as Leffa [51] rely on masks and dense poses that partially leak the original garment, leading to limited gains from FitController. In contrast, FitDiT [15] uses square masks and human keypoints to remove fit cues and thus benefits substantially from FitController, improving all metrics by large margins. These results confirm that FitController enables effective fit-aware VTON while enhancing the overall realism via improved fit consistency.

Fig. 1 presents the qualitative results of FitController on CatVTON [6], and Fig. 5 further shows the results on Leffa and FitDiT. For short-sleeve T-shirts, the generated fits exhibit clear differences in sleeve tightness and torso contour while well preserving garment texture and person identity. For trousers, one can see that *tapered* trousers gradually narrow toward the ankle, and *straight* trousers maintain a uniform leg width. These visualizations intuitively demonstrate that FitController generates perceptually realistic and well-controlled fits for VTON.

5.4. Ablation Study

Condition Injection. We compare our multi-scale fit injector with alternative controlled image generation ap-

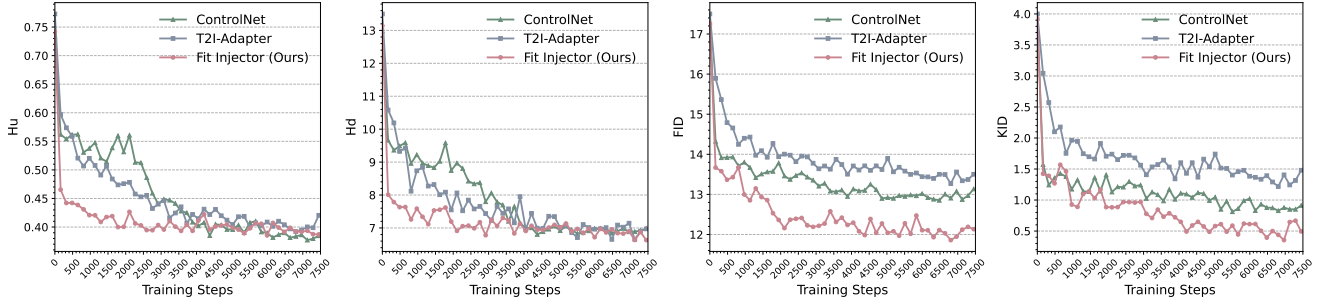


Figure 7. **Training curves of different conditional injection approaches.** Our approach converges faster with superior image quality.

Table 3. Ablation studies on FitController. Best performance is in **boldface**.

(a) **Condition injection.** Comparison of fit injector with alternative injection approaches after 7,500 training steps.

| Method | FID | KID | Hu | Hd | Trainable Params |
|--------------|--------------|-------------|-------------|-------------|------------------|
| ControlNet | 13.14 | 0.91 | 0.38 | 6.98 | 361M |
| T2I-Adapter | 13.50 | 1.48 | 0.42 | 6.97 | 77M |
| Fit Injector | 12.13 | 0.49 | 0.39 | 6.63 | 97M |

(b) **FitController vs. extra training.** FitController accounts for major improvements on Hu and Hd, while extra training (finetune) yields only marginal gains.

| Method | FitCtrl | Finetune | FID | KID | Hu | Hd |
|--------|---------|----------|--------------|-------------|-------------|-------------|
| Leffa | ✗ | ✗ | 18.77 | 2.59 | 0.65 | 10.47 |
| | ✗ | ✓ | 18.69 | 2.18 | 0.63 | 12.67 |
| | ✓ | ✗ | 17.73 | 1.54 | 0.45 | 7.65 |
| FitDiT | ✗ | ✗ | 23.94 | 6.82 | 0.80 | 16.89 |
| | ✗ | ✓ | 19.49 | 3.55 | 0.81 | 14.42 |
| | ✓ | ✗ | 18.48 | 1.86 | 0.46 | 7.94 |

(c) **Training sample size.** FitController trained on 1,000 samples matches full-data performance.

| # Samples | FID | KID | Hu | Hd |
|-------------|--------------|-------------|-------------|-------------|
| 1000 | 17.50 | 1.56 | 0.44 | 8.39 |
| 2000 | 17.51 | 1.42 | 0.44 | 7.21 |
| 3000 | 17.46 | 1.31 | 0.44 | 8.12 |
| 3959 (Full) | 17.80 | 1.52 | 0.45 | 8.25 |

proaches including ControlNet [47] and T2I-Adapter [28] on the short-sleeve T-shirts under the paired setting. Table 3a shows that our fit injector achieves superior generation quality (FID/KID) while maintaining comparable control ability (Hu/Hd) to ControlNet, but with substantially fewer number of parameters. Fig. 7 illustrates the training curves. Our fit injector converges faster and consistently outperforms the baselines in terms of the image quality metrics (FID/KID) throughout the training process. Notably, it can achieve reasonable fit manipulation with only 1,000 training steps.

FitController vs. Extra Training. To verify that the observed performance mainly originates from FitController rather than additional training on Fit4Men, here we conduct an ablation study under the unpaired short-sleeve setting. We compare three configurations: (1) *Baseline*: the original VTON model without both FitController and finetuning; (2) *Backbone finetuning*: finetuning the VTON model on Fit4Men using our garment-agnostic preprocessor, but without FitController; (3) *FitController only*: inserting FitController while freezing the original VTON model. As shown in Table 3b, backbone finetuning slightly improves the FID and KID but has negligible effect on fit control. In contrast, incorporating FitController significantly reduces Hu and Hd, indicating better adherence to the target fit. These results suggest that the performance gains indeed come from FitController. Extra training only contributes to minor image quality improvements.

Training Sample Size. Here we study the impact of training sample size on FitController by training both the layout generator and fit injector with Leffa [51] on the short-sleeve data of varying sample sizes (1,000, 2,000, 3,000, and 3,959 samples) and test under the unpaired setting. According to Table 3c, FitController achieves good performance even with only 1,000 training samples, implying high sample efficiency.

6. Conclusion

We introduced FitController, a novel plug-in module that equips diffusion-based VTON models with precise control over garment fit. It first models garment layouts under specified fit through a fit-aware layout generator conditioned on carefully designed garment-agnostic representations, and then conveys these layout features to VTON models via a multi-scale fit injector, enabling layout-driven generation. In particular, we built a dedicated fit-aware dataset, Fit4Men, and proposed two evaluation metrics specifically tailored to assess fit control. Extensive experiments demonstrate that our approach effectively bridges the gap between high-level fit concepts and realistic try-on image synthesis, providing a practical solution for controllable virtual try-on.

For future work, we plan to extend the framework to a broader range of garment types and fit variations, further enhancing the applicability and generalization of fit-aware virtual try-on systems.

References

[1] Mikołaj Bińkowski, Danica J Sutherland, Michael Arbel, and Arthur Gretton. Demystifying mmd gans. *arXiv preprint arXiv:1801.01401*, 2018. 6

[2] Chieh-Yun Chen, Yi-Chung Chen, Hong-Han Shuai, and Wen-Huang Cheng. Size does matter: Size-aware virtual try-on via clothing-oriented transformation try-on network. In *Proceedings of the IEEE/CVF International Conference on Computer Vision*, pages 7513–7522, 2023. 3

[3] Mengting Chen, Xi Chen, Zhonghua Zhai, Chen Ju, Xuewen Hong, Jinsong Lan, and Shuai Xiao. Wear-any-way: Manipulable virtual try-on via sparse correspondence alignment. In *Proceedings of the European Conference on Computer Vision (ECCV)*, pages 124–142. Springer, 2024. 3

[4] Seunghwan Choi, Sunghyun Park, Minsoo Lee, and Jaegul Choo. Viton-hd: High-resolution virtual try-on via misalignment-aware normalization. In *Proceedings of the IEEE/CVF Conference on Computer Vision and Pattern Recognition*, pages 14131–14140, 2021. 1, 2, 4, 12

[5] Yisol Choi, Sangkyung Kwak, Kyungmin Lee, Hyungwon Choi, and Jinwoo Shin. Improving diffusion models for authentic virtual try-on in the wild. In *Proceedings of the European Conference on Computer Vision (ECCV)*, pages 206–235. Springer, 2024. 2, 6, 7, 13

[6] Zheng Chong, Xiao Dong, Haoxiang Li, Shiyue Zhang, Wenqing Zhang, Xujie Zhang, Hanqing Zhao, Dongmei Jiang, and Xiaodan Liang. Catvton: Concatenation is all you need for virtual try-on with diffusion models. *arXiv preprint arXiv:2407.15886*, 2024. 1, 2, 3, 5, 6, 7, 12, 13

[7] Patrick Esser, Sumith Kulal, Andreas Blattmann, Rahim Entezari, Jonas Müller, Harry Saini, Yam Levi, Dominik Lorenz, Axel Sauer, Frederic Boesel, et al. Scaling rectified flow transformers for high-resolution image synthesis. In *International Conference on Machine Learning*, 2024. 6

[8] Ian Goodfellow, Jean Pouget-Abadie, Mehdi Mirza, Bing Xu, David Warde-Farley, Sherjil Ozair, Aaron Courville, and Yoshua Bengio. Generative adversarial networks. *Communications of the ACM*, 63(11):139–144, 2020. 2

[9] Junhong Gou, Siyu Sun, Jianfu Zhang, Jianlou Si, Chen Qian, and Liqing Zhang. Taming the power of diffusion models for high-quality virtual try-on with appearance flow. In *Proceedings of the 31st ACM International Conference on Multimedia*, pages 7599–7607, 2023. 2

[10] Riza Alp Güler, Natalia Neverova, and Iasonas Kokkinos. Densepose: Dense human pose estimation in the wild. In *Proceedings of the IEEE Conference on Computer Vision and Pattern Recognition*, pages 7297–7306, 2018. 4, 13

[11] Xintong Han, Zuxuan Wu, Zhe Wu, Ruichi Yu, and Larry S Davis. Viton: An image-based virtual try-on network. In *Proceedings of the IEEE/CVF Conference on Computer Vision and Pattern Recognition*, pages 7543–7552, 2018. 2

[12] Martin Heusel, Hubert Ramsauer, Thomas Unterthiner, Bernhard Nessler, and Sepp Hochreiter. Gans trained by a two time-scale update rule converge to a local nash equilibrium. *Advances in Neural Information Processing Systems*, 30, 2017. 6

[13] Ming-Kuei Hu. Visual pattern recognition by moment invariants. *IRE Transactions on Information Theory*, 8(2):179–187, 1962. 5

[14] Daniel P Huttenlocher, Gregory A. Klanderman, and William J Rucklidge. Comparing images using the hausdorff distance. *IEEE Transactions on Pattern Analysis and Machine Intelligence*, 15(9):850–863, 1993. 5

[15] Boyuan Jiang, Xiaobin Hu, Donghao Luo, Qingdong He, Chengming Xu, Jinlong Peng, Jiangning Zhang, Chengjie Wang, Yunsheng Wu, and Yanwei Fu. Fitdit: Advancing the authentic garment details for high-fidelity virtual try-on. *arXiv preprint arXiv:2411.10499*, 2024. 2, 5, 6, 7, 13

[16] Rawal Khirodkar, Timur Bagautdinov, Julieta Martinez, Su Zhaoen, Austin James, Peter Selednik, Stuart Anderson, and Shunsuke Saito. Sapiens: Foundation for human vision models. In *Proceedings of the European Conference on Computer Vision (ECCV)*, pages 206–228, 2024. 13

[17] Jeongho Kim, Guojung Gu, Minho Park, Sunghyun Park, and Jaegul Choo. Stableviton: Learning semantic correspondence with latent diffusion model for virtual try-on. In *Proceedings of the IEEE/CVF Conference on Computer Vision and Pattern Recognition*, pages 8176–8185, 2024. 1, 2, 6, 7, 13

[18] Jeongho Kim, Hoiyeong Jin, Sunghyun Park, and Jaegul Choo. Promptdresser: Improving the quality and controllability of virtual try-on via generative textual prompt and prompt-aware mask. *arXiv preprint arXiv:2412.16978*, 2024. 3

[19] Diederik P Kingma and Max Welling. Auto-encoding variational bayes. *arXiv preprint arXiv:1312.6114*, 2013. 5

[20] Andrea Kollnitz and Marco Pecorari. *Fashion, Performance, and Performativity: The Complex Spaces of Fashion*. Bloomsbury Publishing, 2021. 1

[21] Black Forest Labs. Flux: Official inference repository for flux.1 models, 2024. Accessed: 2024-11-12. 6

[22] Sangyun Lee, Gyojung Gu, Sunghyun Park, Seunghwan Choi, and Jaegul Choo. High-resolution virtual try-on with misalignment and occlusion-handled conditions. In *Proceedings of the European Conference on Computer Vision (ECCV)*, pages 204–219, 2022. 2

[23] Kedan Li, Jeffrey Zhang, Shao-Yu Chang, and David Forsyth. Controlling virtual try-on pipeline through rendering policies. In *Proceedings of the IEEE/CVF Winter Conference on Applications of Computer Vision*, pages 5866–5875, 2024. 3

[24] Yuhan Li, Hao Zhou, Wenxiang Shang, Ran Lin, Xuanhong Chen, and Bingbing Ni. Anyfit: Controllable virtual try-on for any combination of attire across any scenario. *arXiv preprint arXiv:2405.18172*, 2024. 3

[25] Ilya Loshchilov and Frank Hutter. Decoupled weight decay regularization. *arXiv preprint arXiv:1711.05101*, 2017. 6, 12

[26] Davide Morelli, Matteo Fincato, Marcella Cornia, Federico Landi, Fabio Cesari, and Rita Cucchiara. Dress code: High-resolution multi-category virtual try-on. In *Proceedings of the IEEE/CVF Conference on Computer Vision and Pattern Recognition*, pages 2231–2235, 2022. 12

[27] Davide Morelli, Alberto Baldrati, Giuseppe Cartella, Marcella Cornia, Marco Bertini, and Rita Cucchiara. Ladi-vton: Latent diffusion textual-inversion enhanced virtual try-on. In *Proceedings of the 31st ACM International Conference on Multimedia*, pages 8580–8589, 2023. 2

[28] Chong Mou, Xintao Wang, Liangbin Xie, Yanze Wu, Jian Zhang, Zhongang Qi, and Ying Shan. T2i-adapter: Learning adapters to dig out more controllable ability for text-to-image diffusion models. In *Proceedings of the AAAI Conference on Artificial Intelligence*, pages 4296–4304, 2024. 2, 3, 8

[29] Alex Nichol, Prafulla Dhariwal, Aditya Ramesh, Pranav Shyam, Pamela Mishkin, Bob McGrew, Ilya Sutskever, and Mark Chen. Glide: Towards photorealistic image generation and editing with text-guided diffusion models. *arXiv preprint arXiv:2112.10741*, 2021. 3

[30] William Peebles and Saining Xie. Scalable diffusion models with transformers. In *Proceedings of the IEEE/CVF International Conference on Computer Vision*, pages 4195–4205, 2023. 3, 5

[31] Ethan Perez, Florian Strub, Harm De Vries, Vincent Dumoulin, and Aaron Courville. Film: Visual reasoning with a general conditioning layer. In *Proceedings of the AAAI Conference on Artificial Intelligence*, 2018. 5, 12

[32] Dustin Podell, Zion English, Kyle Lacey, Andreas Blattmann, Tim Dockhorn, Jonas Müller, Joe Penna, and Robin Rombach. Sdxl: Improving latent diffusion models for high-resolution image synthesis. *arXiv preprint arXiv:2307.01952*, 2023. 6

[33] Konpat Preechakul, Nattanat Chatthee, Suttisak Wizadwongsu, and Supasorn Suwajanakorn. Diffusion autoencoders: Toward a meaningful and decodable representation. In *Proceedings of the IEEE/CVF Conference on Computer Vision and Pattern Recognition*, pages 10619–10629, 2022. 5

[34] Can Qin, Shu Zhang, Ning Yu, Yihao Feng, Xinyi Yang, Yingbo Zhou, Huan Wang, Juan Carlos Niebles, Caiming Xiong, Silvio Savarese, et al. Unicontrol: A unified diffusion model for controllable visual generation in the wild. *Advances in Neural Information Processing Systems*, 36: 42961–42992, 2023. 3

[35] Alec Radford, Jong Wook Kim, Chris Hallacy, Aditya Ramesh, Gabriel Goh, Sandhini Agarwal, Girish Sastry, Amanda Askell, Pamela Mishkin, Jack Clark, et al. Learning transferable visual models from natural language supervision. In *International Conference on Machine Learning*, pages 8748–8763, 2021. 2

[36] Robin Rombach, Andreas Blattmann, Dominik Lorenz, Patrick Esser, and Björn Ommer. High-resolution image synthesis with latent diffusion models. In *Proceedings of the IEEE/CVF Conference on Computer Vision and Pattern Recognition*, pages 10684–10695, 2022. 3, 5, 6, 12

[37] Siqi Wan, Jingwen Chen, Yingwei Pan, Ting Yao, and Tao Mei. Incorporating visual correspondence into diffusion model for virtual try-on. In *International Conference on Learning Representations*, 2025. 1, 2

[38] Bochao Wang, Huabin Zheng, Xiaodan Liang, Yimin Chen, Liang Lin, and Meng Yang. Toward characteristic-preserving image-based virtual try-on network. In *Proceedings of the European Conference on Computer Vision (ECCV)*, pages 589–604, 2018. 2

[39] Zhou Wang, Alan C Bovik, Hamid R Sheikh, and Eero P Simoncelli. Image quality assessment: from error visibility to structural similarity. *IEEE Transactions on Image Processing*, 13(4):600–612, 2004. 6

[40] Yuhao Xu, Tao Gu, Weifeng Chen, and Arlene Chen. Ootdiffusion: Outfitting fusion based latent diffusion for controllable virtual try-on. In *Proceedings of the AAAI Conference on Artificial Intelligence*, pages 8996–9004, 2025. 2

[41] Yifeng Xu, Zhenliang He, Shiguang Shan, and Xilin Chen. Ctrlora: An extensible and efficient framework for controllable image generation. In *International Conference on Learning Representations*, 2025. 3

[42] Keyu Yan, Tingwei Gao, Hui Zhang, and Chengjun Xie. Linking garment with person via semantically associated landmarks for virtual try-on. In *Proceedings of the IEEE/CVF Conference on Computer Vision and Pattern Recognition*, pages 17194–17204, 2023. 3

[43] Xu Yang, Changxing Ding, Zhibin Hong, Junhao Huang, Jin Tao, and Xiangmin Xu. Texture-preserving diffusion models for high-fidelity virtual try-on. In *Proceedings of the IEEE/CVF Conference on Computer Vision and Pattern Recognition*, pages 7017–7026, 2024. 2

[44] Zhendong Yang, Ailing Zeng, Chun Yuan, and Yu Li. Effective whole-body pose estimation with two-stages distillation. In *Proceedings of the IEEE/CVF International Conference on Computer Vision*, pages 4210–4220, 2023. 13

[45] Ruiyun Yu, Xiaoqi Wang, and Xiaohui Xie. Vtnfp: An image-based virtual try-on network with body and clothing feature preservation. In *Proceedings of the IEEE/CVF International Conference on Computer Vision*, pages 10511–10520, 2019. 2

[46] Winnie Wing-man Yu and L Hunter. *Clothing appearance and fit: Science and technology*. Woodhead publishing, 2004. 1

[47] Lvmin Zhang, Anyi Rao, and Maneesh Agrawala. Adding conditional control to text-to-image diffusion models. In *Proceedings of the IEEE/CVF International Conference on Computer Vision*, pages 3836–3847, 2023. 2, 3, 4, 8

[48] Richard Zhang, Phillip Isola, Alexei A Efros, Eli Shechtman, and Oliver Wang. The unreasonable effectiveness of deep features as a perceptual metric. In *Proceedings of the IEEE/CVF Conference on Computer Vision and Pattern Recognition*, pages 586–595, 2018. 6

[49] Xuanpu Zhang, Dan Song, Pengxin Zhan, Tianyu Chang, Jianhao Zeng, Qingguo Chen, Weihua Luo, and An-An Liu. Boow-vton: Boosting in-the-wild virtual try-on via mask-free pseudo data training. In *Proceedings of the IEEE/CVF Conference on Computer Vision and Pattern Recognition*, pages 26399–26408, 2025. 6

[50] Shihao Zhao, Dongdong Chen, Yen-Chun Chen, Jianmin Bao, Shaozhe Hao, Lu Yuan, and Kwan-Yee K Wong. Uni-controlnet: All-in-one control to text-to-image diffusion models. *Advances in Neural Information Processing Systems*, 36:11127–11150, 2023. 3

- [51] Zijian Zhou, Shikun Liu, Xiao Han, Haozhe Liu, Kam Woh Ng, Tian Xie, Yuren Cong, Hang Li, Mengmeng Xu, Juan-Manuel Pérez-Rúa, et al. Learning flow fields in attention for controllable person image generation. In *Proceedings of the IEEE/CVF Conference on Computer Vision and Pattern Recognition*, pages 2491–2501, 2025. [1](#), [2](#), [5](#), [6](#), [7](#), [8](#), [13](#)
- [52] Luyang Zhu, Dawei Yang, Tyler Zhu, Fitsum Reda, William Chan, Chitwan Saharia, Mohammad Norouzi, and Ira Kemelmacher-Shlizerman. Tryondiffusion: A tale of two unets. In *Proceedings of the IEEE/CVF Conference on Computer Vision and Pattern Recognition*, pages 4606–4615, 2023. [2](#)
- [53] Luyang Zhu, Yingwei Li, Nan Liu, Hao Peng, Dawei Yang, and Ira Kemelmacher-Shlizerman. M&m vto: Multi-garment virtual try-on and editing. In *Proceedings of the IEEE/CVF Conference on Computer Vision and Pattern Recognition*, pages 1346–1356, 2024. [3](#)

FitController: Toward Fit-Aware Virtual Try-On

Supplementary Material

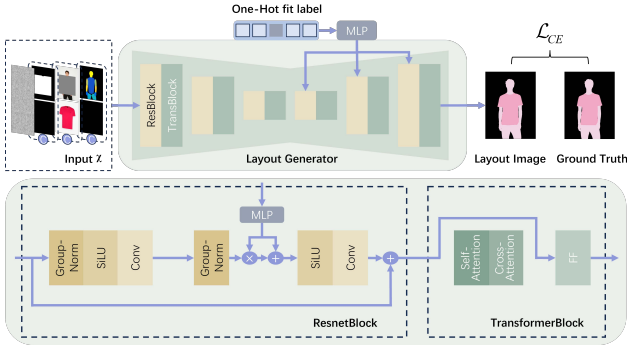


Figure 8. **Overview of Layout Generator.** The layout generator predicts the layout image conditioned on the fit label and is trained with cross-entropy loss.

The supplementary material includes six sections. Sec. A details the fit-aware layout generator. Sec. B provides additional training information for both the layout generator and the fit injector. Sec. C offers a more detailed description of our dataset, Fit4Men. Sec. D presents additional qualitative results generated by FitController. Sec. E reports extended ablation studies on FitController. Finally, Sec. F discusses the limitations of FitController and outlines directions for future work.

A. Details for Fit-Aware Layout Generator

As shown in Fig. 8, we repurpose the U-Net from the Stable Diffusion v1.5 inpainting version [36] as our layout generator. The U-Net takes a 13-channel tensor \mathcal{X} and a one-hot encoded fit label l as input, and generates a 3-channel segmentation map S_l along with fit-aware features C_l . To accommodate our input–output design, we extend its initial convolution layer to 13 channels and modify the output layer to 3 channels. To incorporate l as a control signal, we apply FiLM [31] modulation in each ResNet block to inject the fit information into the decoder features and remove all attention operations from the decoder. Moreover, we extract the features preceding each residual block in the decoder and aggregate them as multi-scale features C_l . The encoder remains unchanged to preserve its semantic representation capability.

B. Training Details

Layout Generator. We expand input channels of the U-Net from 9 to 13 by adding four additional channels for dense pose, which disrupts the pretrained semantic priors in the original U-Net. To recover these semantics, we first



Figure 9. **Limitations of FitController.** FitController occasionally exhibits slight color inconsistencies when generating different fits of the same garment.

modify only the input layer and train a try-on model for 16,000 steps on the VITON-HD dataset following the CatVTON [6] configuration to learn pose encoding.

Next, we freeze the encoder and modify the decoder (without FiLM) and the output layer as described in Sec. A. We train the model for 10,000 steps on the VITON-HD [4] and DressCode [26] datasets for fit-unaware layout prediction.

Finally, we introduce FiLM modulation and fine-tune the decoder on the Fit4Men dataset for 10,000 steps in a fit-aware setting. Both short-sleeve tops and trousers are trained within the same model.

Fit Injector. When applied to different VTON models, we keep the layout generator fixed and train a separate fit injector for each model. For all VTON models as mentioned in Sec. 5.1, the fit injector is trained for 7,500 steps using the MSE loss.

Throughout all stages, we use AdamW [25] with a learning rate of 1×10^{-5} and a batch size of 64.

C. Details for Fit4Men

We construct a dataset, Fit4Men, for fit-aware VTON. As shown in Fig. 10, it contains 5,000 pairs of men’s short-sleeve shirts with three fit types (slim, regular, and loose) and 8,000 pairs of men’s trousers with two fit types (tapered and straight). The dataset is divided into training and test sets with a ratio of 4 : 1. To simulate real-world try-on scenarios, Fit4Men features various camera distances, model orientations, and pose complexities.



Figure 10. **Overview of Fit4Men.** (a) and (b) present the statistical distributions of the training and testing sets. (c) illustrates representative examples of five garment fit types, supporting our fit-aware training objective. (d) shows samples captured at different camera distances, while (e) and (f) depict variations in model orientations and poses, respectively, ensuring the diversity and robustness of Fit4Men.

Camera Distance. Fit4Men covers a wide range of camera distances to reflect variations commonly seen in fashion photography. We categorize them into three levels: proximal, intermediate, and distant. Proximal views capture only a specific region, such as the upper or lower body; intermediate views display the full body within the frame; while distant views are taken from farther away, presenting the model with noticeable spatial separation from the camera. This diversity enables robust performance under varying framing conditions.

Model Orientation. The dataset includes models captured from multiple orientations to enhance spatial robustness. Specifically, each subject may appear in frontal, lateral, or rear views, covering a complete range of typical fashion poses. Such variation ensures that models trained on Fit4Men can generalize to arbitrary viewing angles during virtual try-on generation.

Pose Complexity. To capture realistic human dynamics, Fit4Men introduces three levels of pose complexity: simple, moderate, and complex. Simple poses refer to upright standing positions with no limb occlusion; moderate poses involve partial self-occlusion, such as crossed arms or bent legs; and complex poses depict dynamic or non-standing states, such as sitting or running. This variety allows evaluating how well VTON models preserve garment fit consistency under different body configurations.

For annotations, we employ DWPose [44] to extract human keypoints, DensePose [10] for dense pose, and Sapiens [16] for ground-truth segmentation maps.

D. Additional Qualitative Results

We provide additional qualitative comparisons to further demonstrate the effectiveness and generality of the proposed FitController across different diffusion-based VTON models, including CatVTON [6], Leffa [51], FitDiT [15], IDM-VTON [5], and StableVITON [17]. Figures 12–16 present results on short-sleeve shirts, illustrating how FitController enables precise and continuous control over garment tightness (*i.e.*, *slim*, *regular*, and *loose* fits). Figures 17–20 show analogous results on trousers, verifying that our module generalizes well to other garment categories while maintaining consistent fit-aware behavior across models.

E. Ablation Study

Garment-Agnostic Preprocessor. Fig. 11 compares the results of FitController trained with commonly used garment-agnostic representations versus our proposed ones. When trained with the conventional representations, FitController tends to preserve the original garment shape and fails to adjust the fit according to the given label. In contrast, our garment-agnostic preprocessor allows FitController to

generate images that accurately reflect the specified fit conditions. These results demonstrate the effectiveness of our design and its suitability for fit-aware VTON.

Effect of Semantic Priors for the Layout Generator. We examine whether incorporating semantic priors benefits the layout generator. Without semantic priors, the layout generator is randomly initialized; with them, it is initialized using pretrained diffusion weights. As shown in Table 4, the diffusion-based initialization consistently improves all metrics, indicating that semantic knowledge from pretrained diffusion models facilitates more accurate body–garment segmentation and enhances try-on performance.

F. Limitations and Future Work

In practical applications, we occasionally observe color inconsistencies across generated results of different fits for the same garment, as illustrated in Fig. 9. This issue primarily arises from inherent biases in the training data: due to variations in lighting conditions and imaging setups, the garment color in product images often differs slightly from that in try-on images. As a result, the model may inadvertently learn this bias and produce garments with slightly darkened or lightened colors during generation.

Moreover, our current dataset focuses on menswear and includes only two garment categories—short-sleeve shirts and trousers—thus covering a limited range of fit types. Future work will extend the dataset to womenswear and incorporate a wider variety of garment categories and fit styles, aiming to improve the diversity and generalization of fit-aware VTON systems.

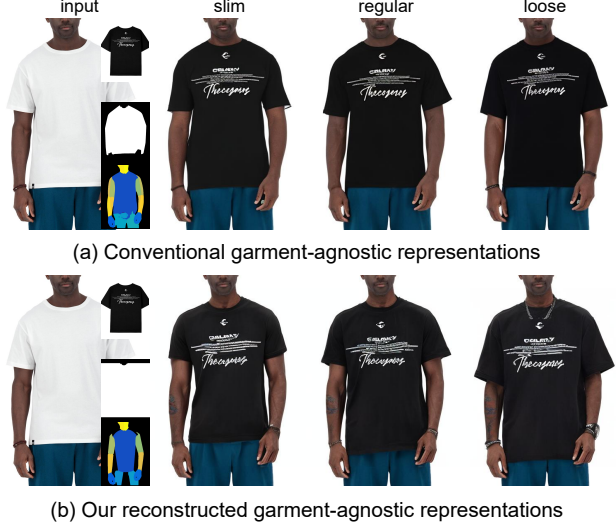


Figure 11. **Ablation study on the garment-agnostic preprocessor.** (a) FitController trained with commonly used garment-agnostic representations. (b) FitController trained with our proposed representations. Our method enables more faithful fit-aware control and better garment adaptation.

Table 4. Ablation on semantic priors for the layout generator. Initializing the layout generator with pretrained diffusion weights (semantic prior) yields better try-on performance.

| Semantic Prior | FID \downarrow | KID \downarrow | Hu \downarrow | Hd \downarrow |
|------------------------------|------------------|------------------|-----------------|-----------------|
| Without Prior (Random Init.) | 13.35 | 1.11 | 0.41 | 7.91 |
| With Diffusion Prior | 12.45 | 0.62 | 0.40 | 7.05 |

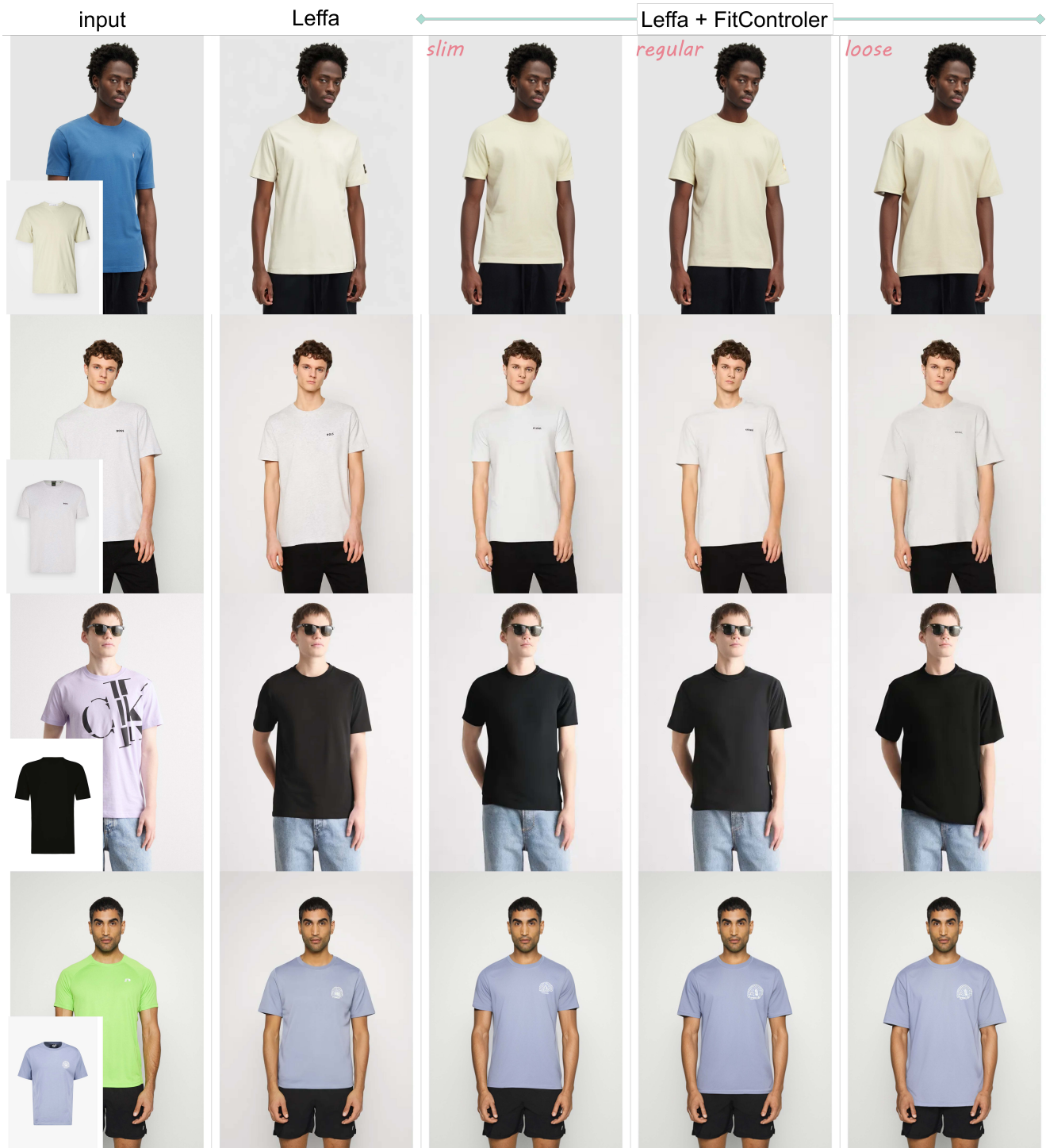


Figure 12. **Sample generated by Leffa without and with FitController on short-sleeve shirts.** FitController provides reliable fit control and maintains high visual fidelity for a wide range of poses.



Figure 13. **Sample generated by FitDiT without and with FitController on short-sleeve shirts.** FitController provides reliable fit control and maintains high visual fidelity for a wide range of poses.

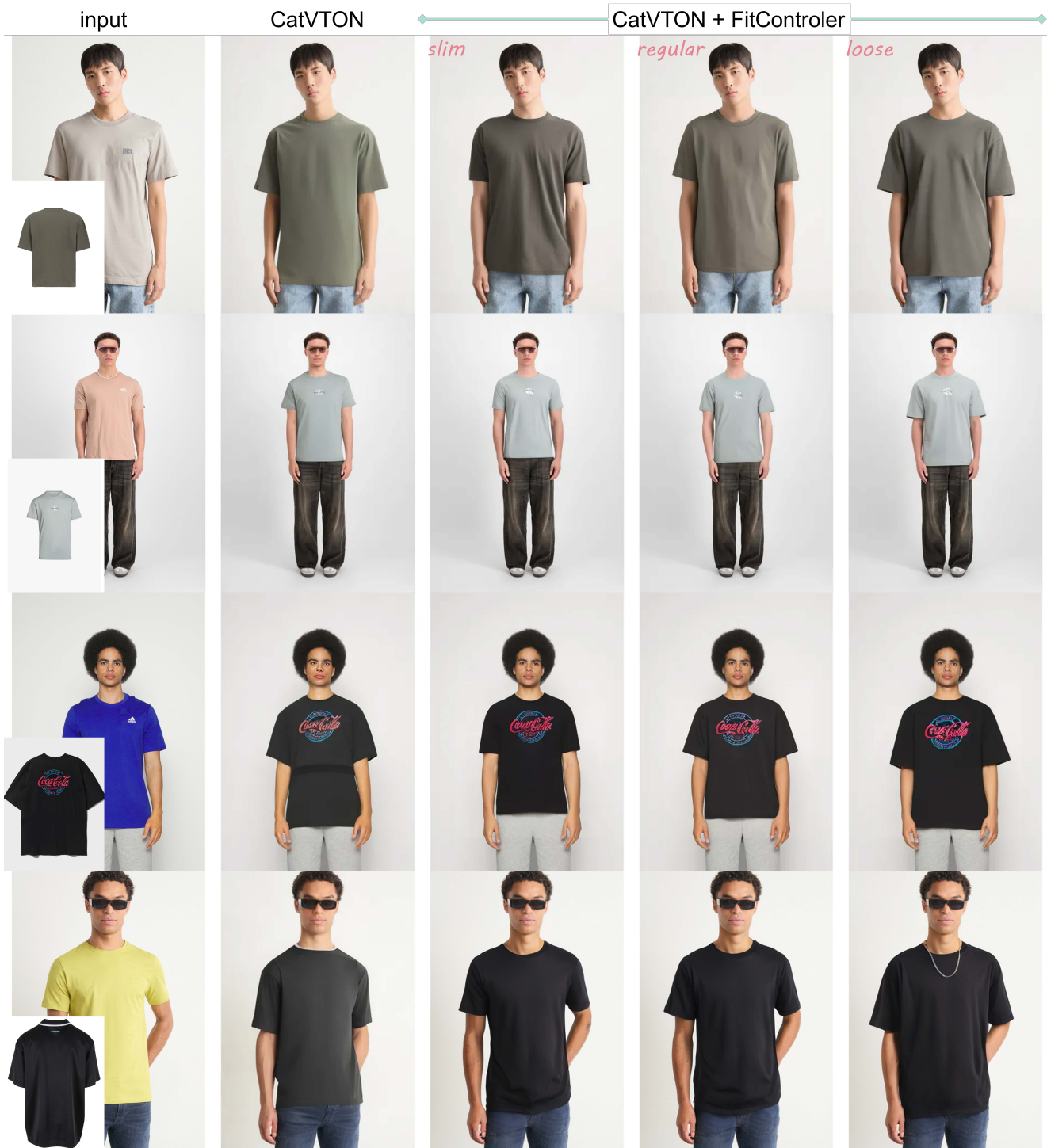


Figure 14. **Sample generated by CatVTON without and with FitController on short-sleeve shirts.** FitController provides reliable fit control and maintains high visual fidelity for a wide range of poses.

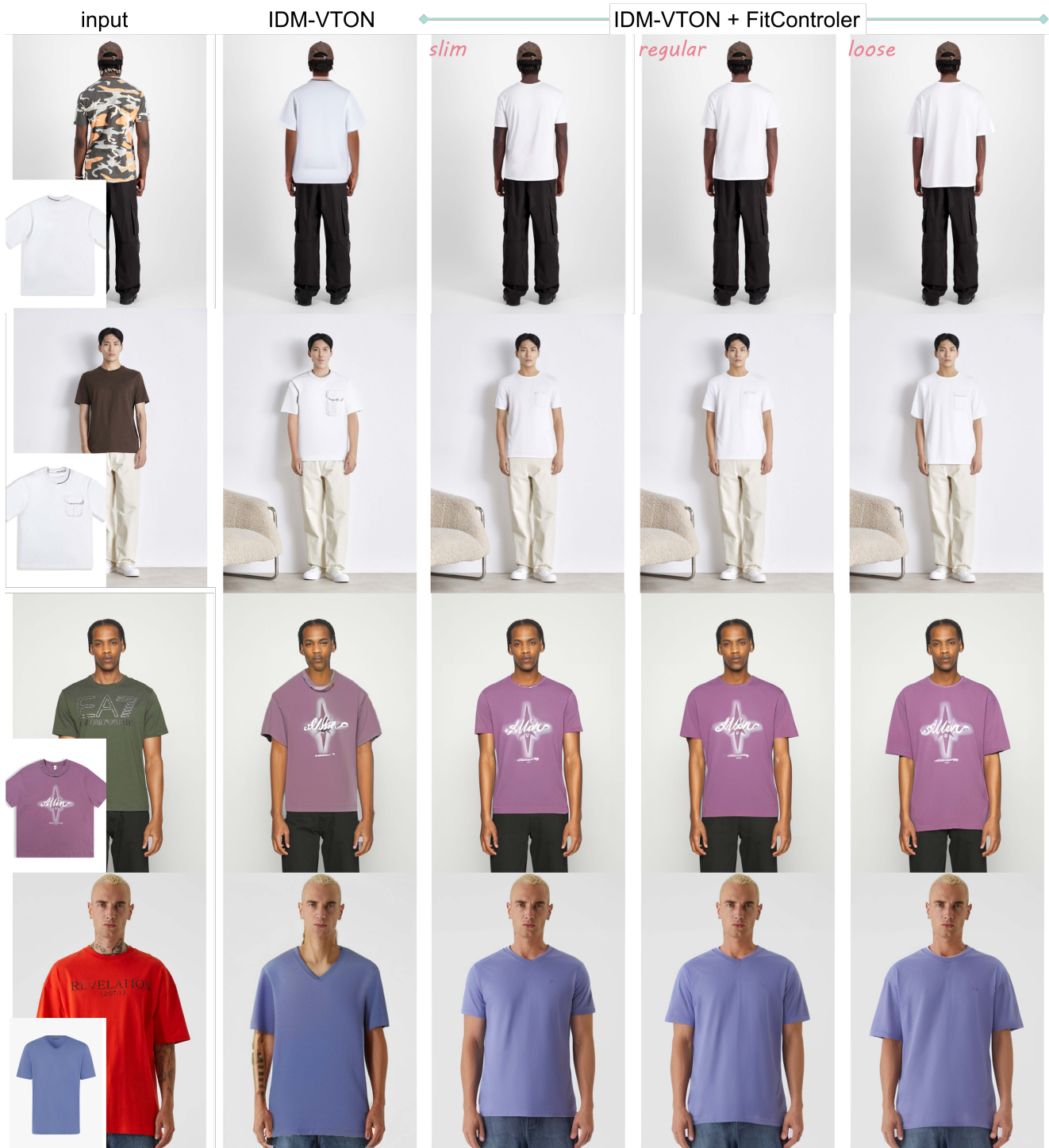


Figure 15. **Sample generated by IDM-VTON without and with FitController on short-sleeve shirts.** FitController provides reliable fit control and maintains high visual fidelity for a wide range of poses.



Figure 16. **Sample generated by StableVITON without and with FitController on short-sleeve shirts.** FitController provides reliable fit control and maintains high visual fidelity for a wide range of poses.

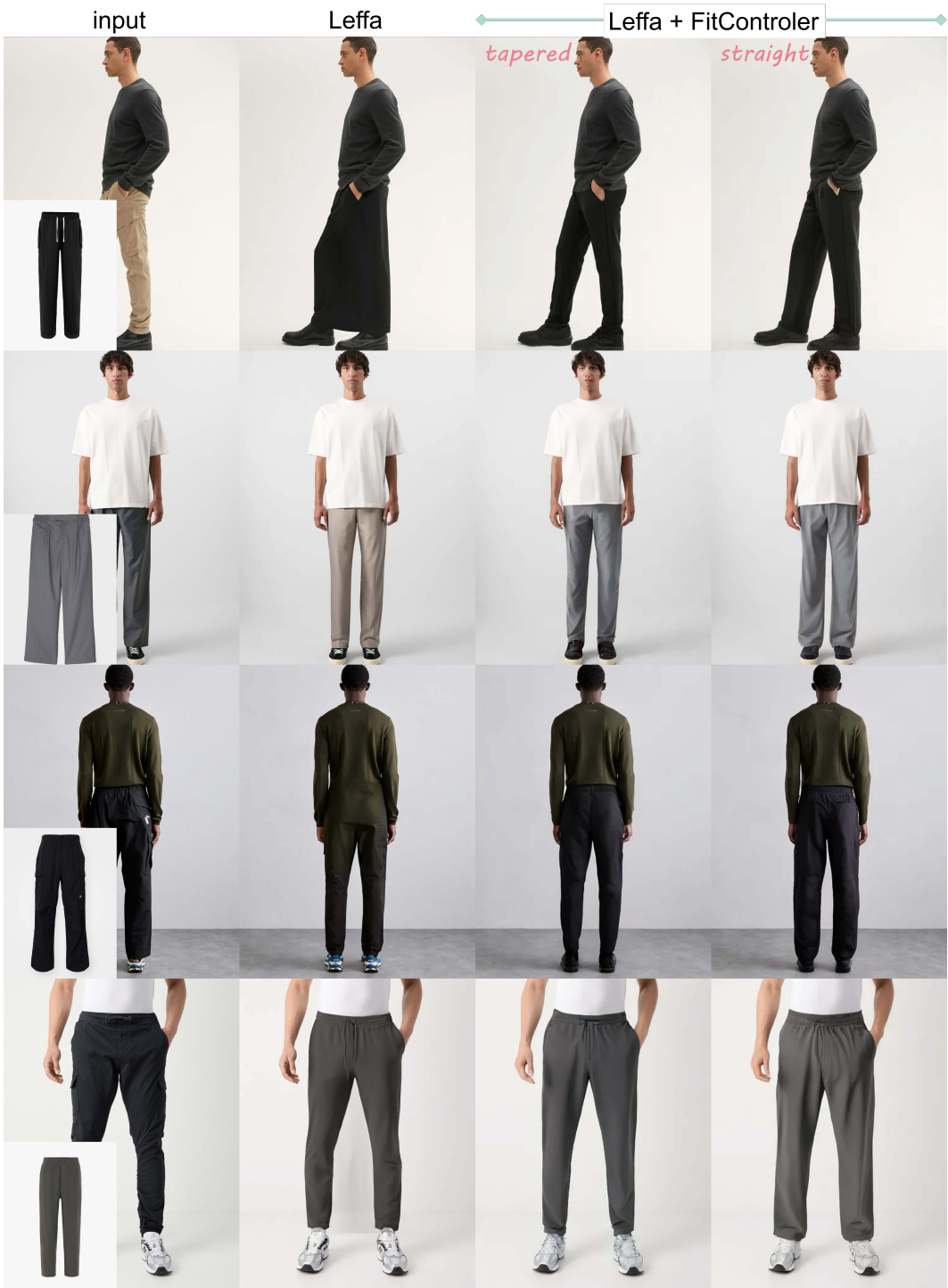


Figure 17. **Sample generated by Leffa without and with FitController on trousers.** FitController provides reliable fit control and maintains high visual fidelity for a wide range of poses.



Figure 18. **Sample generated by FitDiT without and with FitController on trousers.** FitController provides reliable fit control and maintains high visual fidelity for a wide range of poses.

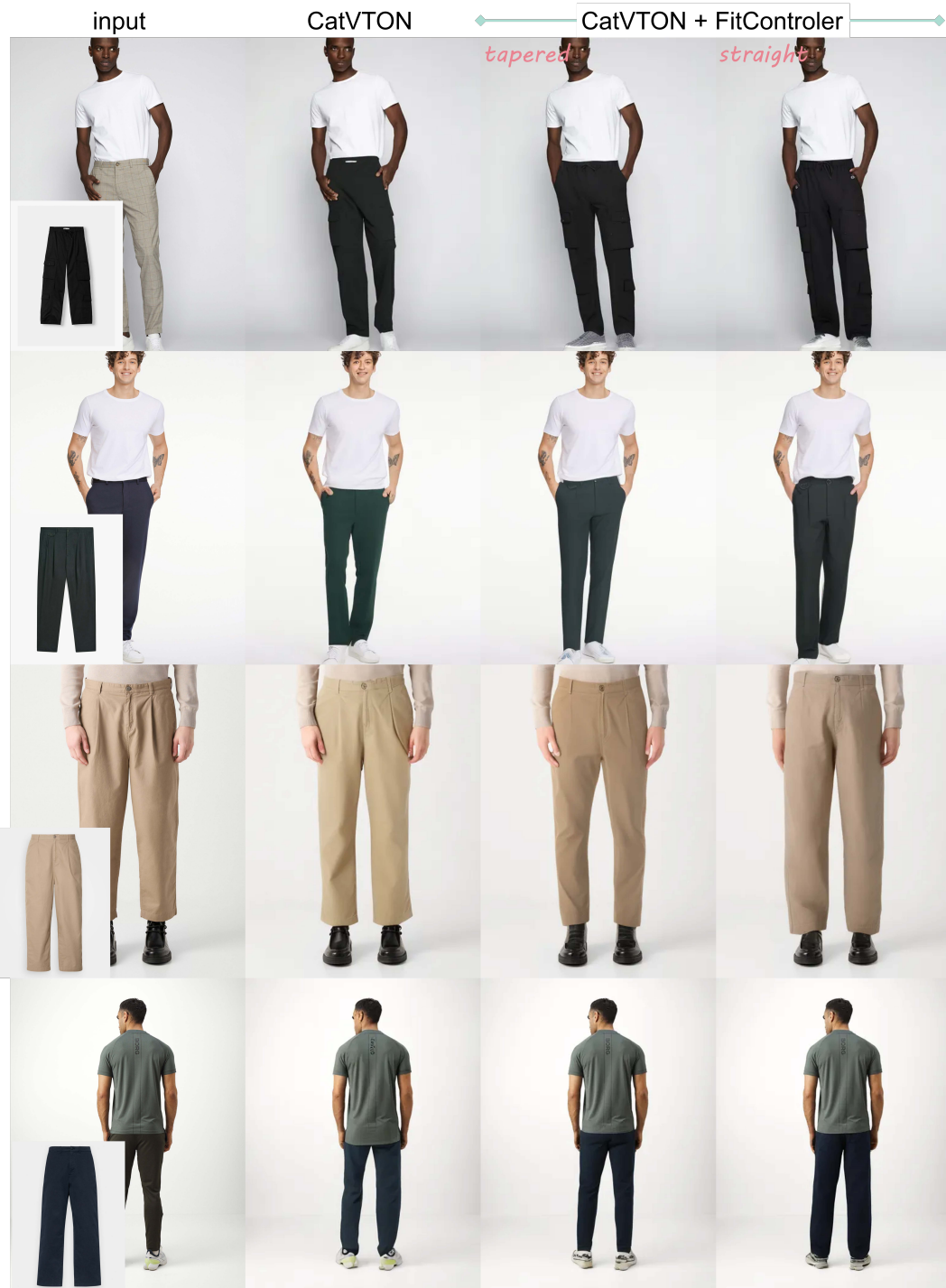


Figure 19. **Sample generated by CatVTON without and with FitController on trousers.** FitController provides reliable fit control and maintains high visual fidelity for a wide range of poses.

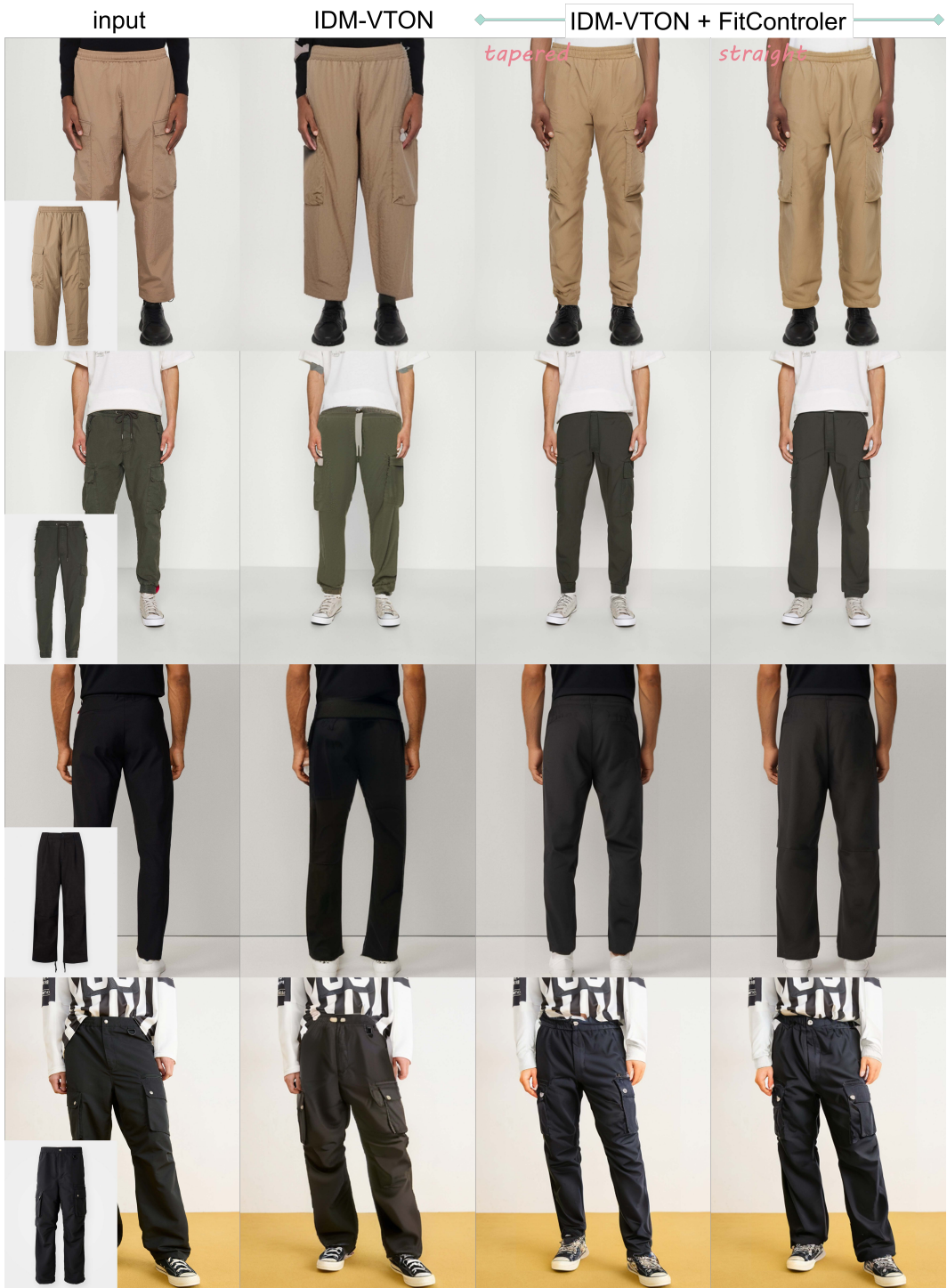


Figure 20. **Sample generated by IDM-VTON without and with FitController on trousers.** FitController provides reliable fit control and maintains high visual fidelity for a wide range of poses.